Angewandte Chemie
Eine Zeitschrift der Gesellschaft Deutscher Chemiker

Supporting Information

Encapsulation of an Au_{25} Nanocluster inside a Porphyrin Nanoring Enhances Singlet Oxygen Generation and Photo-Electrocatalytic CO_2 Reduction

A. Ziarati, H. Gotfredsen, A. Rosspeintner, J. Zhao, H. L. Anderson*, T. Bürgi**

Supporting Information for

Encapsulation of an Au_{25} Nanocluster inside a Porphyrin Nanoring Enhances Singlet Oxygen Generation and Photo-Electrocatalytic CO_2 Reduction

Abolfazl Ziarati,[+*1] Henrik Gotfredsen,[+2] Arnulf Rosspeintner,[1] Jiangtao Zhao,[1] Harry L. Anderson,[*2] and Thomas Bürgi[*1]

[+] These authors contributed equally to this work.

1. Department of Physical Chemistry, University of Geneva, 30 Quai Ernest-Ansermet, 1211 Geneva (Switzerland)

2. Department of Chemistry, University of Oxford, Chemistry Research Laboratory, Oxford OX1 3TA, (UK)

*Correspondence to: Abolfazl.Ziarati@unige.ch, Harry.Anderson@chem.ox.ac.uk, Thomas.Buergi@unige.ch

Table of Contents

General methods

All chemicals were purchased from commercial suppliers and used without any further treatment.

Synthesis of Porphyrin nanorings

Porphyrin nanorings ***c*-P6**, [1] ***c*-P8**, [2] and ***c*-P10** [3] were prepared analogously to already published procedures.

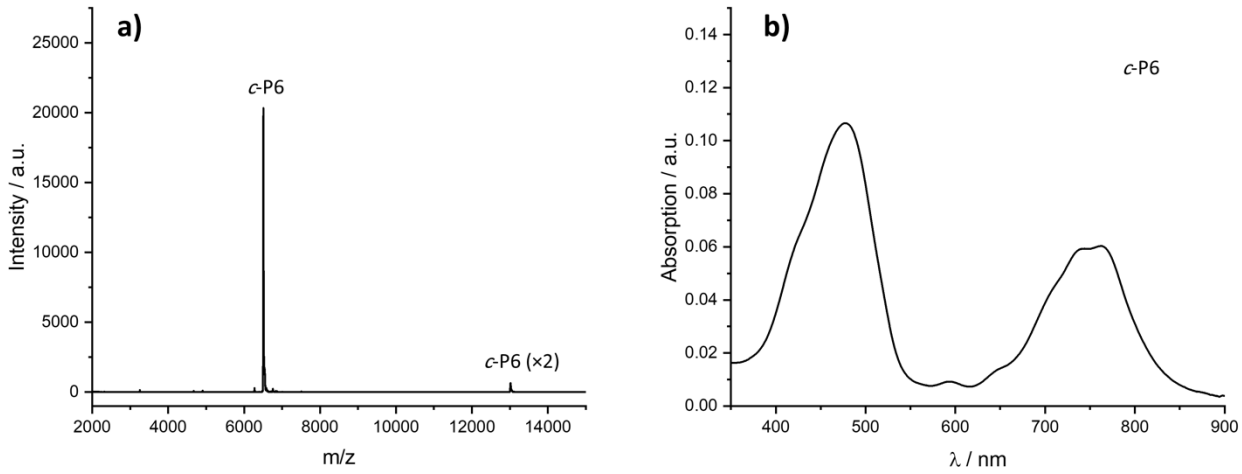

Figure S1. (a) MALDI-MS of ***c*-P6** and (b) UV-vis absorption spectrum of ***c*-P6** in chloroform. The peaks at *m/z* = 6507.8 (calculated 6508.4) in MALDI-MS is assigned to the ***c*-P6** and the peak located at *m/z* = 13015.6 is related to its double mass.

Synthesis of $Au_{25}PyET_{18}Na$ Cluster

The **$Au_{25}PyET_{18}Na$** cluster salt was synthesized according to the literature with some modifications. [4]
The synthesis involved adding a solution of 4-pyridylethanemercaptan (PyET, 8 mL, 100 mM in MeOH; 0.8 mmol) dropwise into a solution of $HAuCl_4 \cdot 3H_2O$ (24 mL, 6.7 mM in THF; 0.16 mmol) in a 100 mL-round-bottom flask. The mixture underwent a transition from a light reddish cloudy suspension to a white cloudy suspension during the addition of PyET. After overnight stirring, white residues adhered to the flask's inner wall were completely dispersed by sonication for 1 min, forming a turbid suspension again. Subsequently, freshly prepared $NaBH_4$ aqueous solution (1.6 mL, 1.0 M, 1.6 mmol; prepared by dissolving 189.2 mg of $NaBH_4$ in 5 mL ice-cold MilliQ water) was rapidly added to the suspension under vigorous stirring, turning the suspension black to indicate the formation of Au_m clusters. After approximately 1 h of vigorous stirring, the color became slightly brownish. The stirring rate was decreased to 500 rpm, allowing the etching process to continue for at least 48 h. During the prolonged etching process, the color of the solution gradually changed to dark brown, suggesting the conversion of crude polydisperse Au_m clusters to monodisperse **$Au_{25}PyET_{18}$** clusters. The crude sample was initially cleaned by centrifugation to remove any solids. Then, under stirring, aqueous HCl (2 mL, 375.0 mM) was rapidly added to the crude sample, and the brownish precipitation was collected by centrifugation. The collected solid was washed twice with THF and then redissolved in MeOH (8 mL). The insoluble particles were removed by centrifugation. Aqueous NaOH solution (32 mL, 200.0 mM) was added to the resulting 8 mL of Au_{25}-containing MeOH solution, deprotonating the pendant pyridine groups and simultaneously precipitating the **$Au_{25}PyET_{18}Na$** clusters. Finally, the brown solid, collected by centrifugation, was washed thrice with water, dried under reduced pressure, and stored in the freezer.

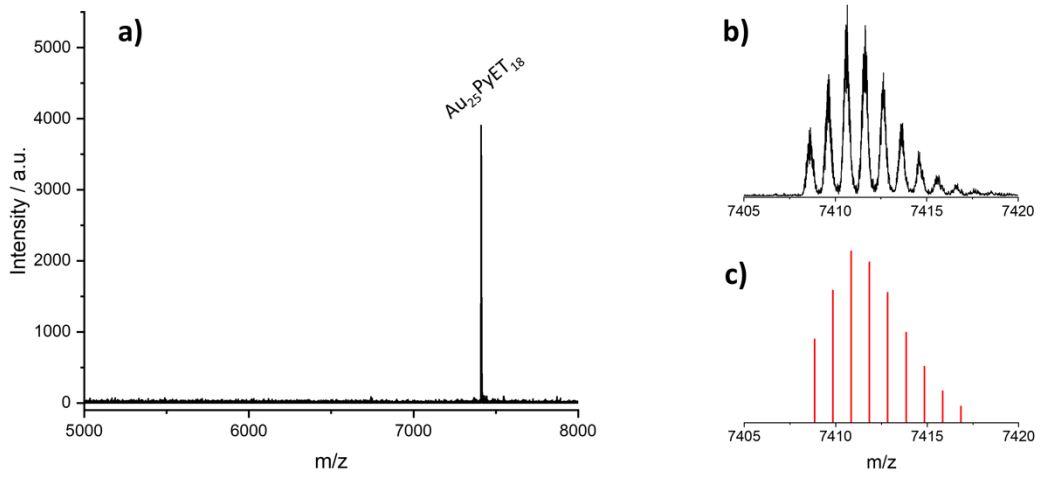

Figure S2. (a) Negative mode high-resolution electrospray ionization mass spectra (HRESI-MS) of **$Au_{25}PyET_{18}Na$** and (b) comparison of experimental and (c) simulated isotopic patterns of **$Au_{25}PyET_{18}Na$**. The peak at *m/z* = 7410.65 (calculated 7410.84), corresponding to [**$Au_{25}PyET_{18}$**]$^{-}$.

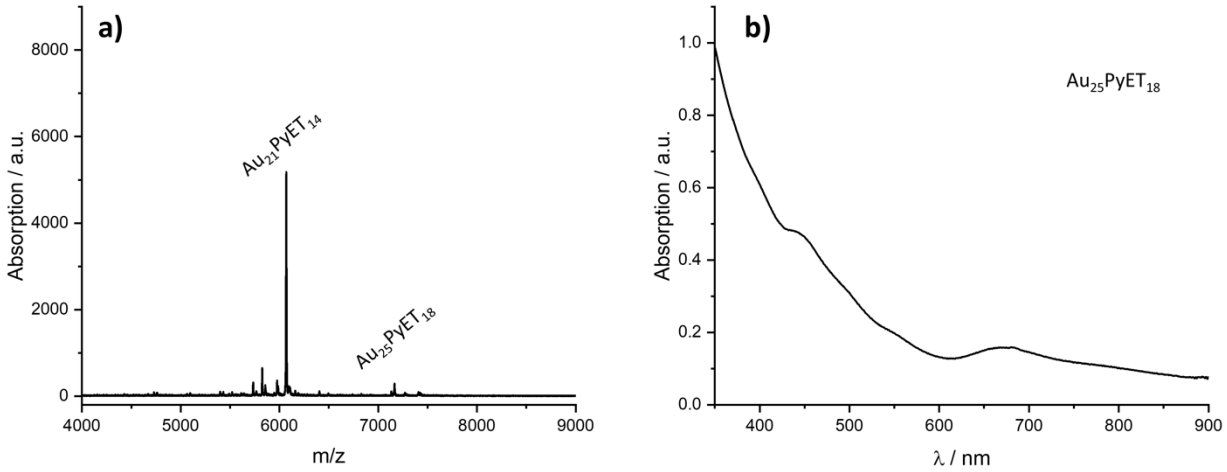

Figure S3. (a) Positive mode MALDI-MS of **$Au_{25}PyET_{18}Na$** and (b) UV-vis absorption spectrum of **$Au_{25}PyET_{18}Na$** in MeOH. The MALDI-MS results exhibited a clear peak at *m/z* = 6068.7 (calculated 6070.8), attributed to cluster following the loss of four gold atoms and 4 PyET ligands (Au_4PyET_4). Such fragmentation is a common occurrence for Au clusters during MS analysis. [5] The UV-vis absorption spectra of the product exhibited a broad band around 670 nm and a distinct absorption around 450 nm, confirming the successful synthesis of **$Au_{25}PyET_{18}^{-}$** nanoclusters. [4]

Synthesis of $Au_{25}PET_{18}$ nanoclusters

The $Au_{25}PET_{18}$ clusters were synthesized were prepared according to the literature. [6]

Typically, $HAuCl_4 \cdot 3H_2O$ (1.00 g, 2.54 mmol) and TOABr (1.67 g, 3.05 mmol) were dissolved in THF (250 mL) and vigorously stirred for about 15 min (orange-red color solution was obtained). Next, 2-phenylethanethiol (1.7 mL, 12.68 mmol) was added dropwise to the stirring solution, during which the solution gradually changed color from orange-red to yellow. The solution was left to stir for about 2 h until the solution became colorless. Then, 25 mL of a freshly prepared ice-cold aqueous solution of $NaBH_4$ (0.96 g, 25.4 mmol, 10 equiv.) was rapidly poured at once into the rapidly stirred reaction mixture. An immediate outgassing was observed, and the solution changed color to brown-black. The reaction was left to stir for about 40 h. The reaction mixture was filtered on a filter paper to remove insoluble complexes. The filtrate was concentrated under reduced pressure to yield a thick orange oil, and was subsequently exposed to an extensive washing procedure in order to remove of unreacted thiol and other precursors. First, ~300 mL of MeOH was poured into the flask and was left to stand for a few hours until a brown precipitate formed. The supernatant was carefully decanted, and the precipitate was dissolved in toluene. Subsequently, the toluene was evaporated under reduced pressure. To the crude product a fresh portion of MeOH was added and the above procedure was repeated several times until all free thiols were removed. The purification and isolation of the Au_{25} clusters was done using size-exclusion chromatography (SEC) in dichloromethane. During the synthetic reaction and later separation procedure both negatively charged and neutral Au_{25} clusters were formed. To transform the $[Au_{25}PET_{18}]^-$ $[TOA]^+$ into $[Au_{25}PET_{18}]^0$ clusters, the former were dissolved in dichloromethane and passed over a silica gel column. The eluted green color solution was dried under reduced pressure and was stored in the freezer.

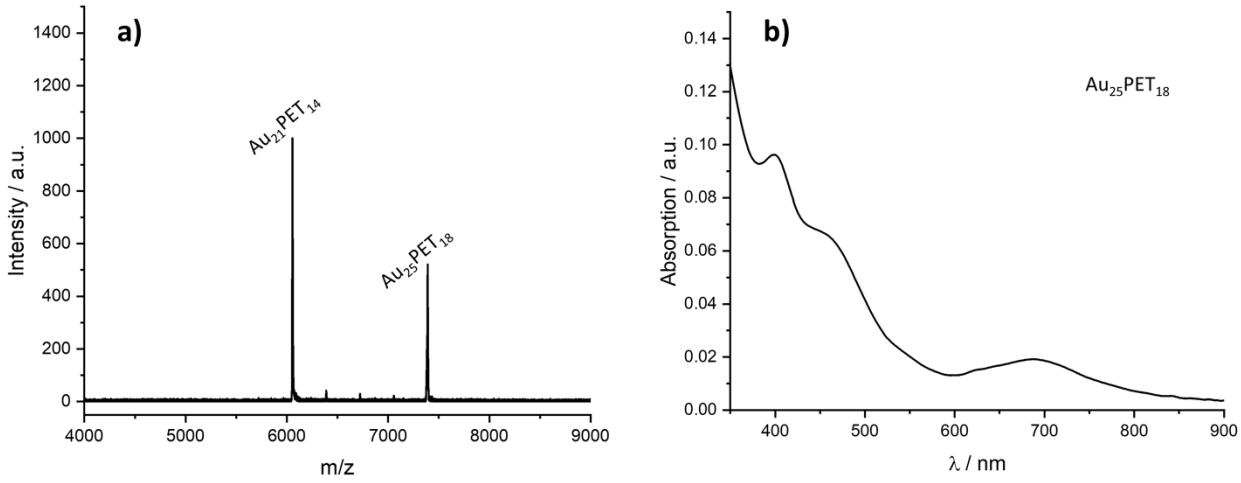

Figure S4. (a) MALDI-MS of $Au_{25}PET_{18}$ and (b) UV-vis absorption spectrum of $Au_{25}PET_{18}$ in chloroform.

Characterization

Molecular mechanics modelling was carried out with the MM+ force field in Hyperchem™ 8.0.10 (Hypercube Inc.) package.

Optical spectroscopic measurements were conducted in HPLC grade solvents using quartz cuvettes (10 mm path length, Starna Scientific Ltd, UK). UV-vis-NIR absorption spectra were acquired on a Perkin Elmer Lambda 20 spectrometer at 298 K, with temperature control by a PTP-1 Peltier unit from Perkin Elmer or on a JASCO V-670 spectrophotometer. Fluorescence spectra were acquired at 298 K using an Edinburgh Instruments FS5 spectrofluorometer using Fluoracle® software. The instrument is equipped with a xenon arc lamp (providing 230–1000 nm excitation range), a thermostatic sample holder (SC-20) and both an R13456 PMT detector (200–950 nm spectral coverage, Hamamatsu) and an InGaAs analogue NIR detector (850–1650 nm spectral coverage). High-resolution (HR) ESI-MS was studied by QSTAR Pulsar (QqTOF) instrument, with negative polarity. MALDI-MS analysis was performed on Bruker AutoFlex spectrometer equipped with a 337 nm nitrogen laser with positive polarity. The matrix applied is trans-2-[3-(4- tert-butylphenyl)-2-methyl-2-propenylidene]-malononitrile. 3.5 mg of matrix was dissolved in 100 μL dichloromethane. Matrix and sample were mixed at ratio 1:1 and 2 μL of the mixture was dropped on a MALDI plate and air-dried. Gas products and liquid products were identified and quantified by gas chromatography (SCION-456 GC) and H-NMR (400 MHz, Bruker), respectively, indicating that CO and H_2 are the only products. No liquid products were detected. pH was measured by pH meter (FE20/EL20, Mettler-Toledo). Time-resolved photoluminescence was conducted with a pulsed laser excitation at λ = 440 nm using a home-built time-correlated single photon counting set-up described in Ref. [7]

Molecular modelling

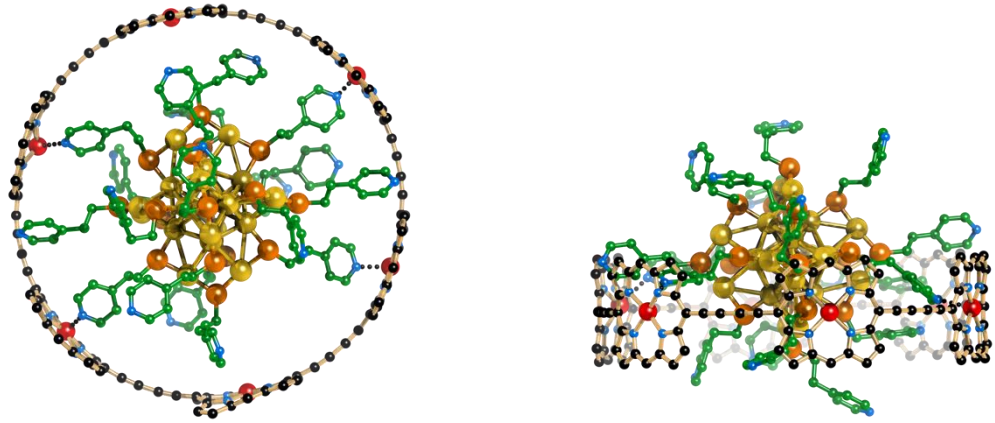

Figure S5. Molecular mechanics+ model of the ***c*-P6•Au$_{25}$PyEt$_{18}^-$** complex. Mean N–Zn coordinate bond length = 2.43 Å based on the four shortest coordinate bonds. By comparison, it is 2.15 Å in the ***c*-P6•T6** crystal structure. [8]

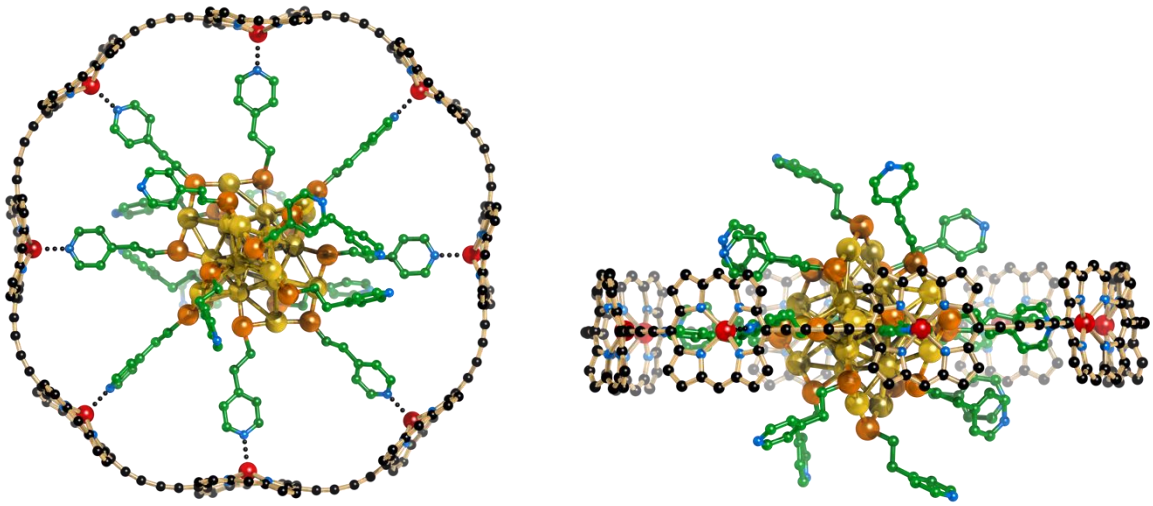

Figure S6. Molecular mechanics+ model of the ***c*-P8•Au$_{25}$PyEt$_{18}^-$** complex. Mean N–Zn coordinate bond length = 2.46 Å based on the eight shortest coordinate bonds.

Table S1. Measured distances in ***c*-P*N*** and model complexes ***c*-P*N*•Au$_{25}$PyEt$_{18}^-$** (N = 6 and 8).

	***c*-P6**	***c*-P8**	***c*-P6•Au$_{25}$PyEt$_{18}$**	***c*-P8•Au$_{25}$PyEt$_{18}$**
Averaged Zn–Zn diameter ($d_{c\text{-}PN}$) / Å	25.6	34.3	25.5 (+0.6)	30.3 (–3.3)
†Ideal Zn–Zn diameter for bound ring complex / Å	24.9	33.6	-	-
‡Ideal template/guest diameter for ***c*-P*N*** / Å	21.2	29.9	-	-
Averaged N–N diameter in Au$_{25}$PyEt$_{18}$ (bound to ***c*-P*N***) / Å	-	-	21.0 (–0.2)	23.2 (–6.0)
Au$_{25}$S$_{18}$ core off-set from ***c*-P*N*** plane / Å	-	-	3.33	0.01

† $d_{Zn–Zn,\ bound} = d_{c\text{-}PN} - 2\cdot(0.37\ Å)$

‡ $d_{Template,\ ideal} = d_{c\text{-}PN} - 2\cdot(2.16\ Å + 0.37\ Å)$

The N(pyridine)–Zn(porphyrin) coordinate bond length is 2.16 Å and the distance by which the zinc atom moves out of the plane of the porphyrin when it becomes 5-coordinate is 0.37 Å. [8]

Binding experiments

All titrations were carried out in $CDCl_3$ at 298 K. The purchased $CDCl_3$ was filtered through a plug of neutral alumina before use. For each titration, the concentration of porphyrin was kept constant to avoid dilution effects, by adding porphyrin to the ligand solution. It was necessary to use methanol for dissolving the **$Au_{25}PyET_{18}Na$** gold cluster due to its low solubility in chloroform. As a result, about 0–0.9 % methanol by volume was added to the cuvette during a formation titration, while 0.05–0.1% of methanol by volume was present at the starting point of a knock-out titration.

The formation constants (K_f) for gold cluster binding to the nanorings were determined by fitting the binding isotherms to a 1:1 binding model using the equation:

$$A = \frac{\left(K_f([P]_0 + [L]) + 1\right) - \sqrt{\left(K_f([P]_0 + [L] + 1)\right)^2 - 4K_f[P]_0[L]}}{2K_f[P]_0} \cdot \left(A_f - A_0\right) + A_0$$

where A, is the observed absorption at a specific wavelength or the difference of absorbance between two wavelengths, A_0 is the starting absorption at this wavelength, A_f is the asymptotic final absorption at this wavelength, $[L]$ is the concentration of the ligand, and $[P]_0$ is the concentration of the porphyrin host. The fitting analyses were carried out using the non-linear curve fitting tool in OriginPro 2022.

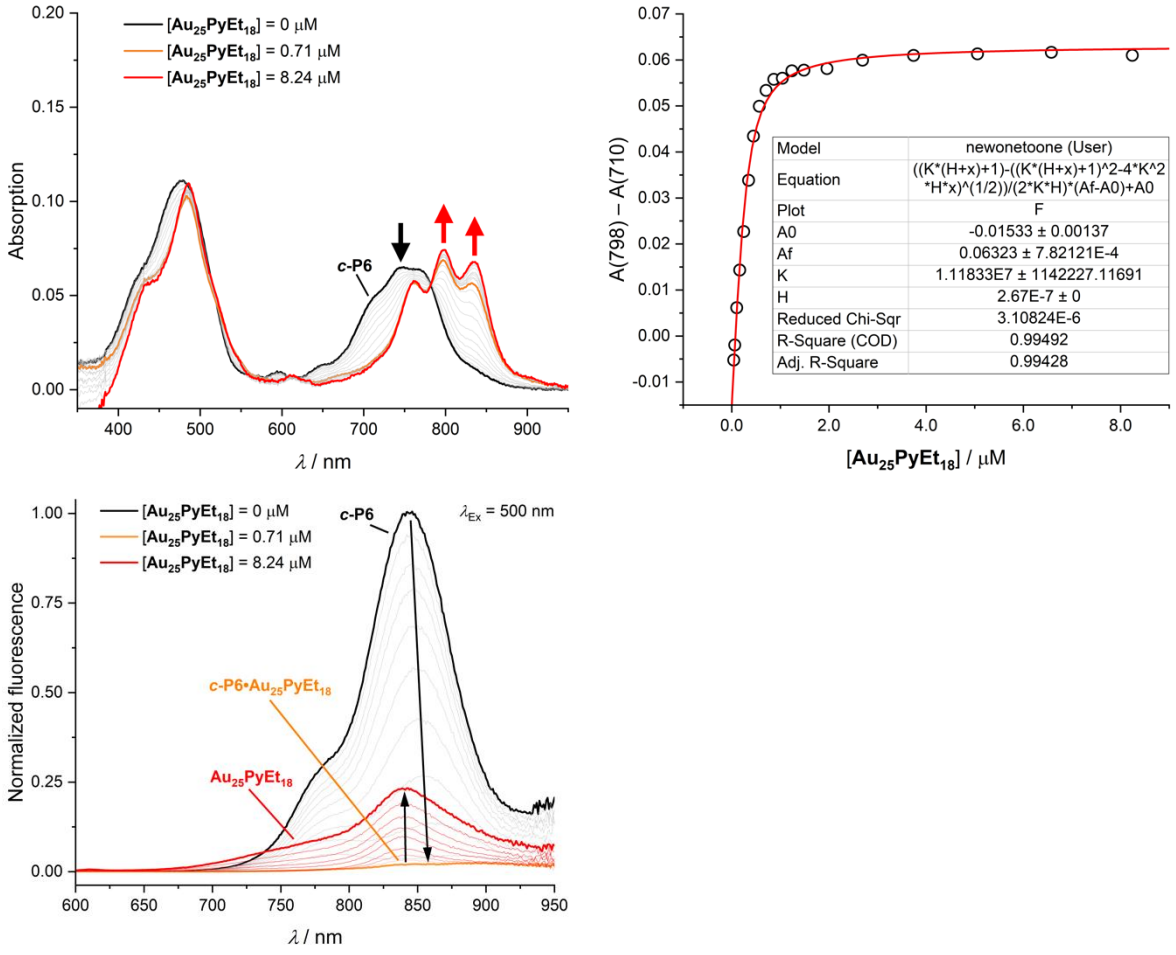

Figure S7. Formation titration between ***c*-P6** and **$Au_{25}PyET_{18}Na$** measured in parallel by absorption and fluorescence, ($CDCl_3$ + 0–0.9% MeOH, 298 K, [***c*-P6**] = $2.67 \cdot 10^{-7}$ M). The absorption contribution of **$Au_{25}PyET_{18}Na$** has been subtracted from the absorption titration. A binding isotherm from the change of absorption was fitted to a one-to-one binding model, yielding a formation constant $K_f = 1.1 \cdot 10^7$ M^{-1} ($R^2 = 0.994$). Quenching efficiency is 97% based on integration.

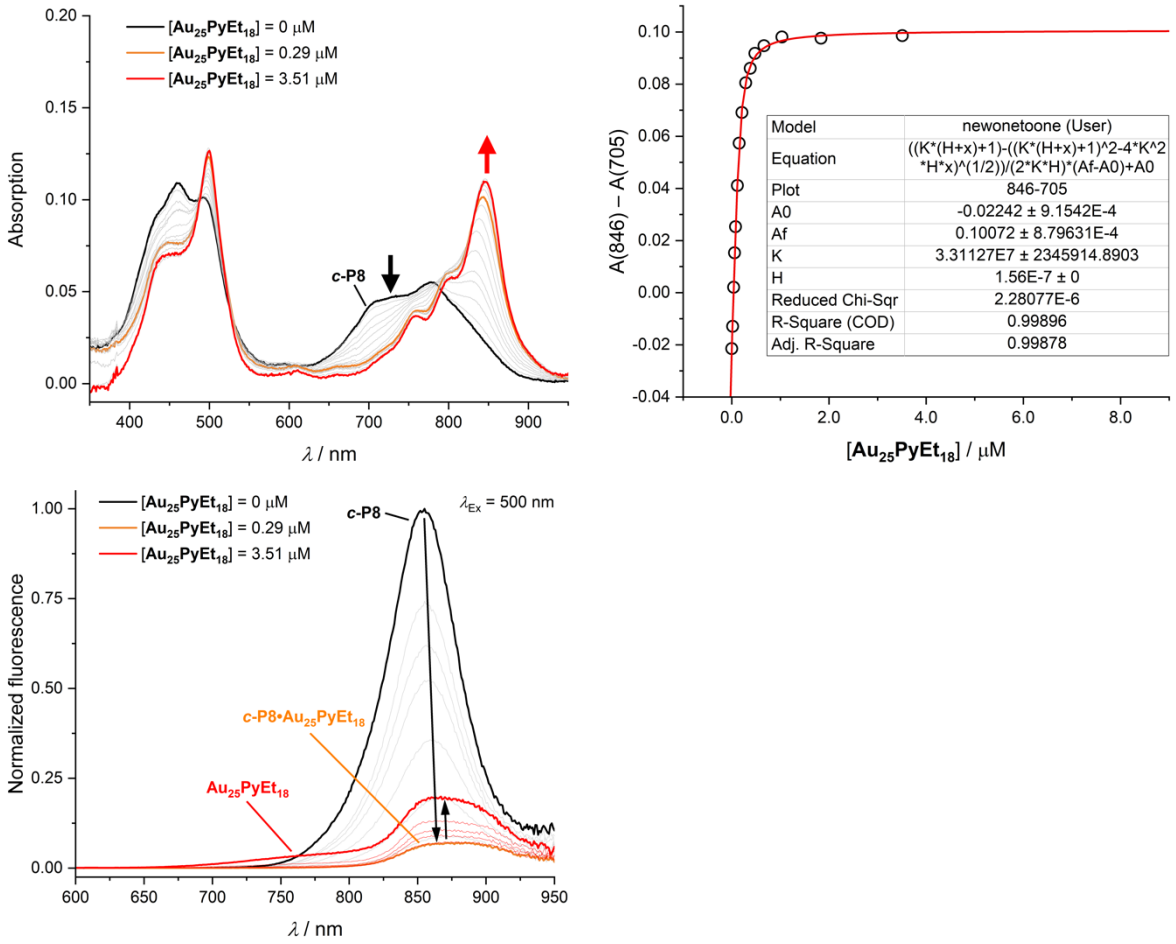

Figure S8. Formation titration between ***c*-P8** and **Au$_{25}$PyET$_{18}$Na** measured in parallel by absorption and fluorescence, ($CDCl_3$ + 0–0.4% MeOH, 298 K, [***c*-P8**] = $1.56 \cdot 10^{-7}$ M). The absorption contribution of **Au$_{25}$PyET$_{18}$Na** has been subtracted from the absorption titration. A binding isotherm from the change of absorption was fitted to a one-to-one binding model, yielding a formation constant $K_f = 3.1 \cdot 10^7$ M^{-1} ($R^2 = 0.999$). Quenching efficiency is 91% based on integration.

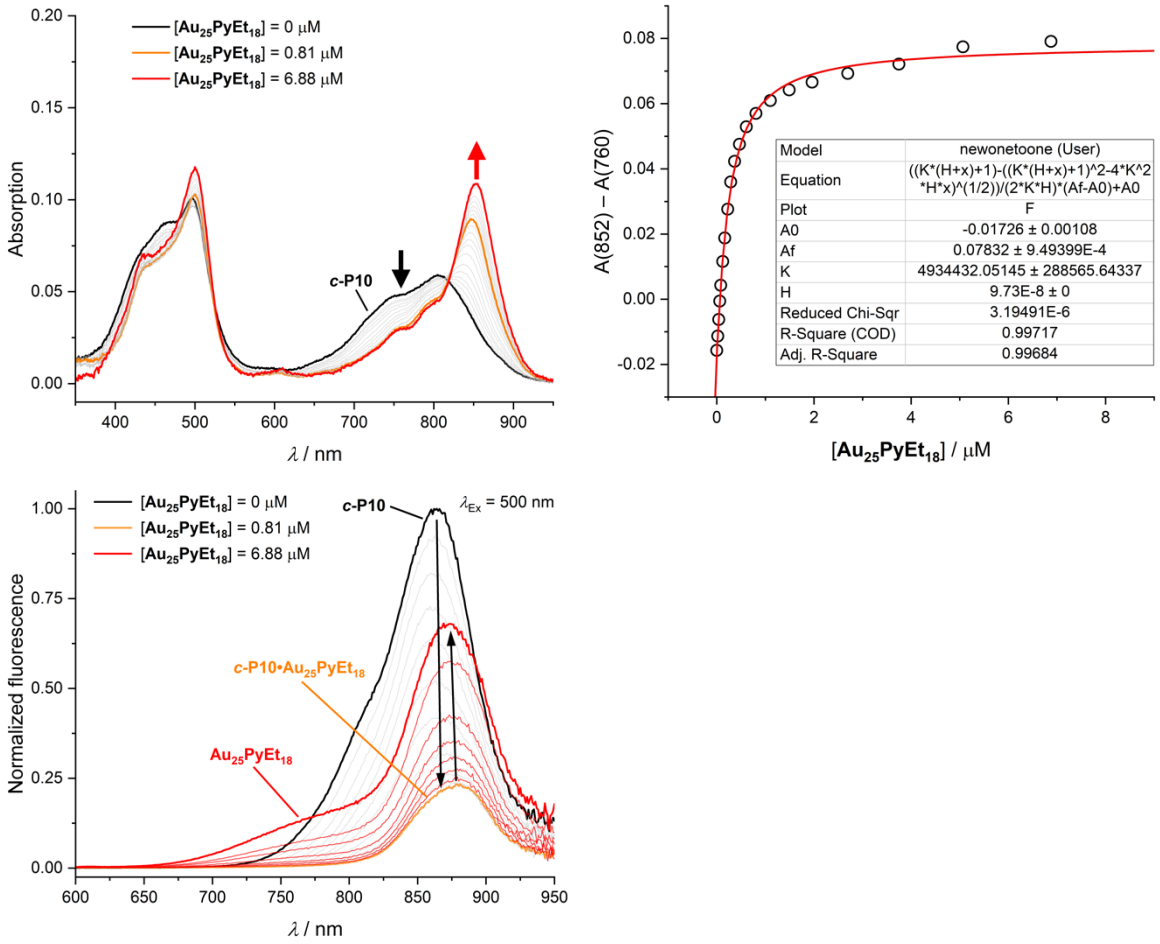

Figure S9. Formation titration between ***c*-P10** and **Au$_{25}$PyET$_{18}$Na** measured in parallel by absorption and fluorescence, ($CDCl_3$ + 0–0.8% MeOH, 298 K, [***c*-P10**] = $9.73 \cdot 10^{-8}$ M). The absorption contribution of **Au$_{25}$PyET$_{18}$Na** has been subtracted from the absorption titration. A binding isotherm from the change of absorption was fitted to a one-to-one binding model, yielding a formation constant $K_f = 4.9 \cdot 10^6$ M^{-1} ($R^2 = 0.997$). Quenching efficiency is 80% based on integration.

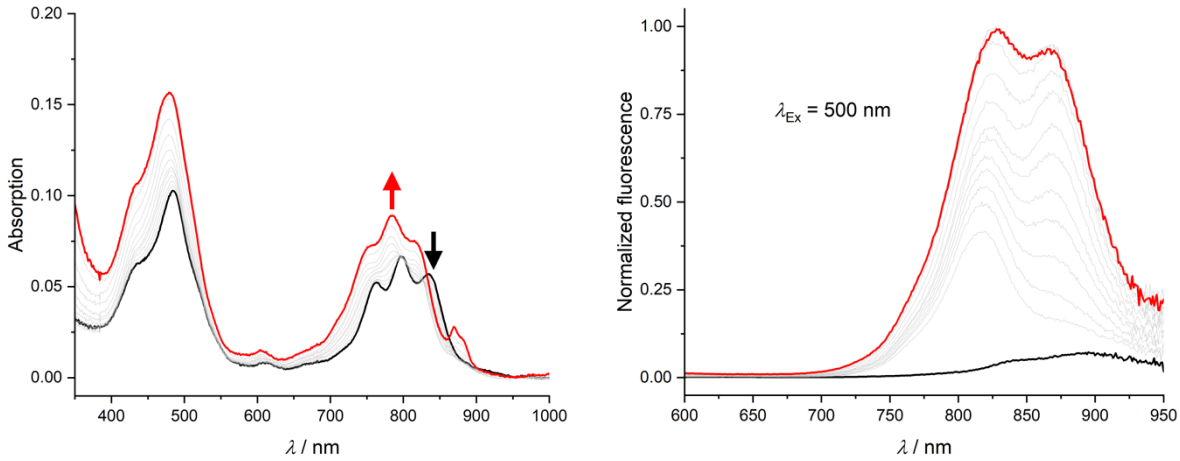

Figure S10. Knock-out titration of ***c*-P6•Au$_{25}$PyET$_{18}$Na** with pyridine ($CDCl_3$ + 0.05-0.1% MeOH, 298 K, [***c*-P6•Au$_{25}$PyET$_{18}^-$**] = $2.67 \cdot 10^{-7}$ M) measured in parallel by absorption (left) and fluorescence (right). Starting point in black ([pyridine] = 0 M) and end point in red ([pyridine] = 3.63 M).

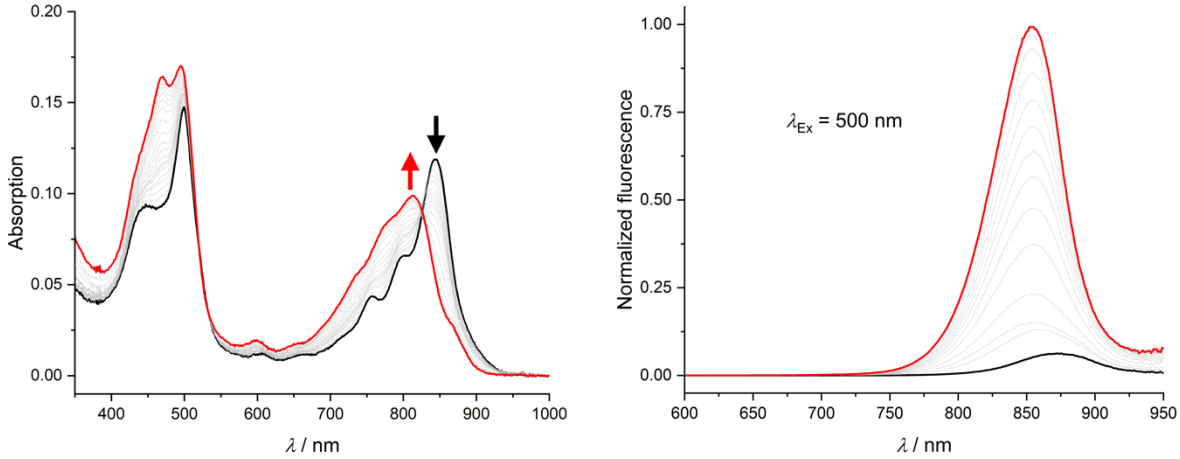

Figure S11. Knock-out titration of ***c*-P8•Au$_{25}$PyET$_{18}$Na** with pyridine ($CDCl_3$ + 0.05-0.1% MeOH, 298 K, [***c*-P8•Au$_{25}$PyET$_{18}$Na**] = $1.45 \cdot 10^{-7}$ M) measured in parallel by absorption (left) and fluorescence (right). Starting point in black ([pyridine] = 0 M) and end point in red ([pyridine] = 0.86 M).

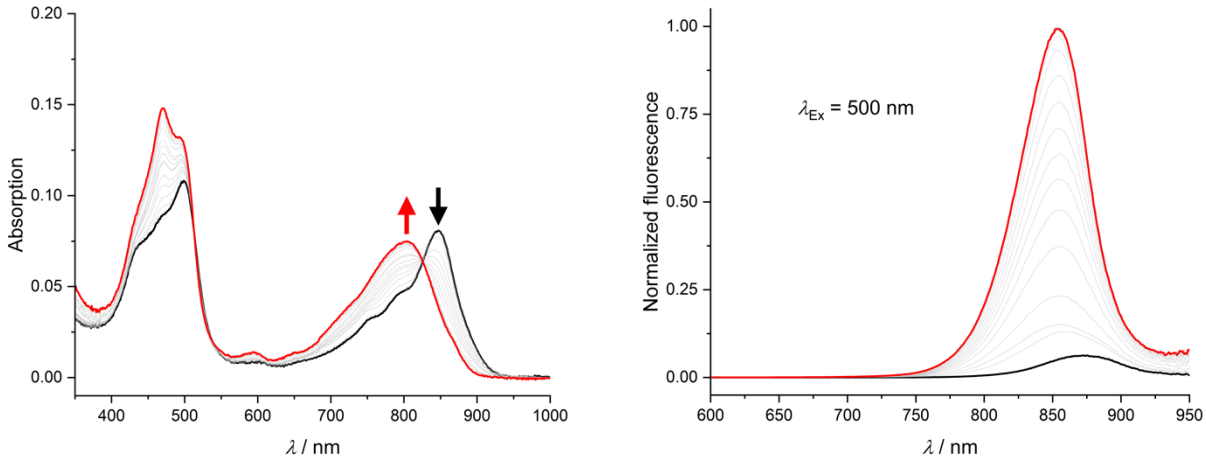

Figure S12. Knock-out titration of ***c*-P10•Au$_{25}$PyET$_{18}$Na** with pyridine ($CDCl_3$ + 0.05-0.1% MeOH, 298 K, [***c*-P10•Au$_{25}$PyET$_{18}$Na**] = $9.73 \cdot 10^{-8}$ M) measured in parallel by absorption (left) and fluorescence (right). Starting point in black ([pyridine] = 0 M) and end point in red ([pyridine] = 1.02 M).

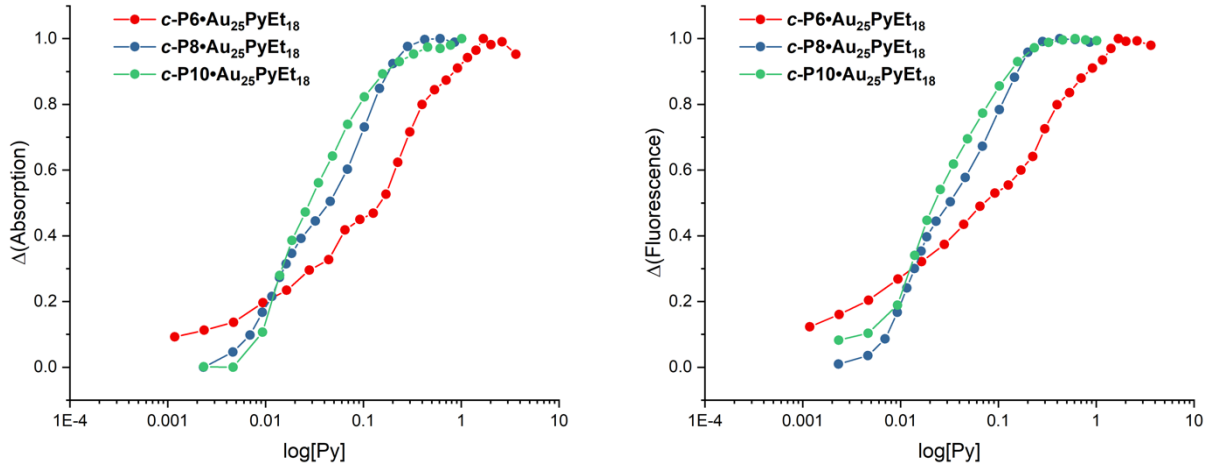

Figure S13. Summary of knock-out titrations measured in parallel by absorption (left) and fluorescence (right). The change in Q-band absorption as a result of knock-out is plotted as Δ(Absorption) = $A_{785} - A_{845}$ (for $N = 6$), $\Delta A = A_{770} - A_{842}$ (for $N = 8$), and $\Delta A = A_{804} - A_{847}$ (for $N = 10$). The change in fluorescence as a result of knock-out is plotted as Δ(Fluorescence) at the fluorescence maxima of the free nanorings, which is 867 nm (for $N = 6$), 864 nm (for $N = 8$), and 854 nm (for $N = 10$).

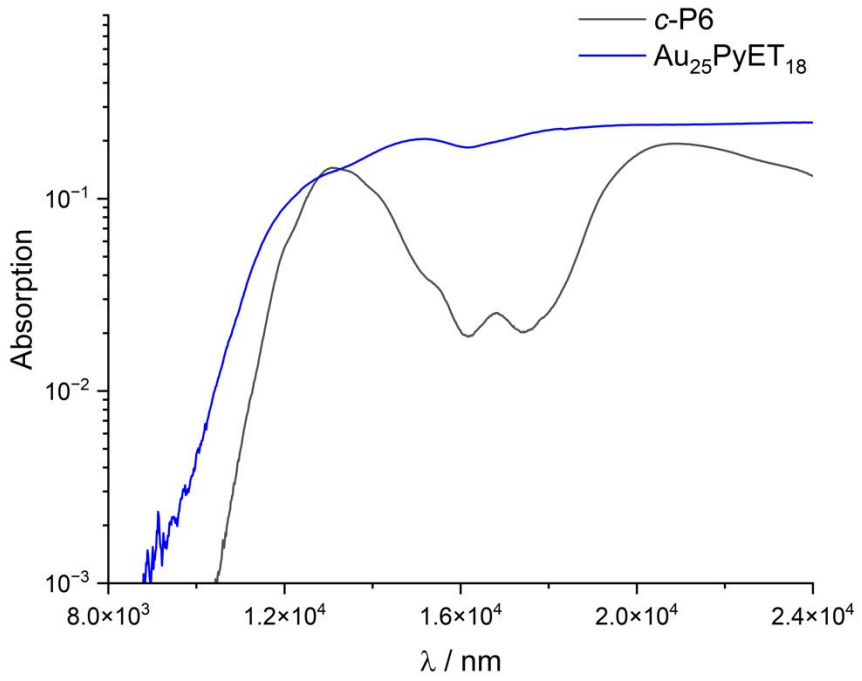

Figure S14. Comparison of the absorption spectra of ***c*-P6** and $\mathbf{Au_{25}PyET_{18}^{-}}$.

a)

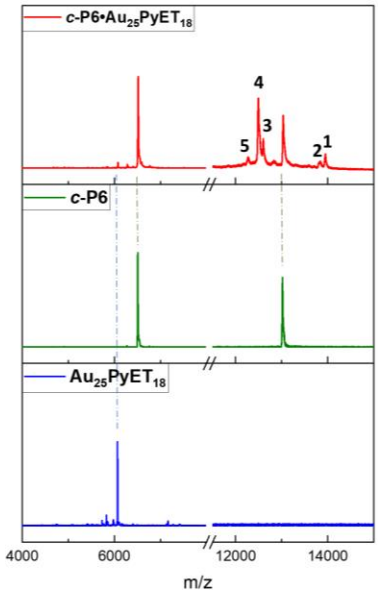

b)

Peak	Experimental Mass	Calculated Mass	Assigned Structure
1	13941.4	13943.3	*c*-P6•$Au_{25}PyET_{18}$(Na)
2	13835.6	13837.1	*c*-P6•$Au_{25}PyET_{17}$(Na)S
3	12601.1	12602.6	*c*-P6•$Au_{21}PyET_{14}$(Na)
4	12494.8	12496.4	*c*-P6•$Au_{21}PyET_{13}$(Na)S
5	12266.3	12267.4	*c*-P6•$Au_{20}PyET_{13}$(Na)

Figure S15. MALDI-MS of assembly (**$Au_{25}PyET_{18}Na$** and ***c*-P6**). Investigation of the mass spectroscopy of ***c*-P6•$Au_{25}PyET_{18}^-$** assembly (a) indicates appearing of some new peaks in the range of m/z= 12000 to m/z= 14000, specifically, the peak at *m/z* = 13941.4 and *m/z* = 12601.1 can be assigned to the ***c*-P6•$Au_{25}PyET_{18}^-$**, and ***c*-P6•$Au_{25}PyET_{18}^-$** after losing Au_4PyET_4, respectively. This identification was further confirmed by comparing the observed peaks with calculated ones (b).

a)

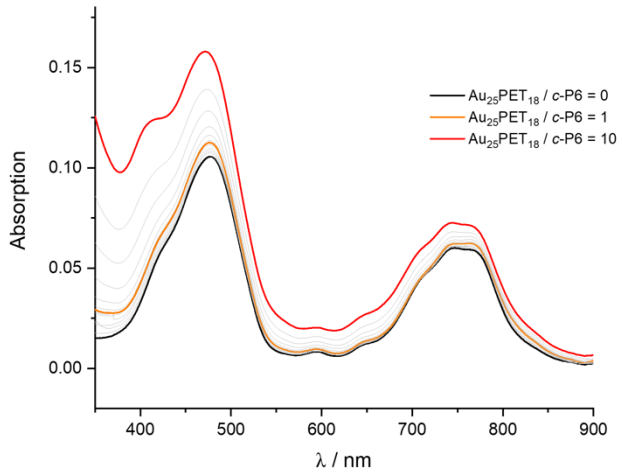

b)

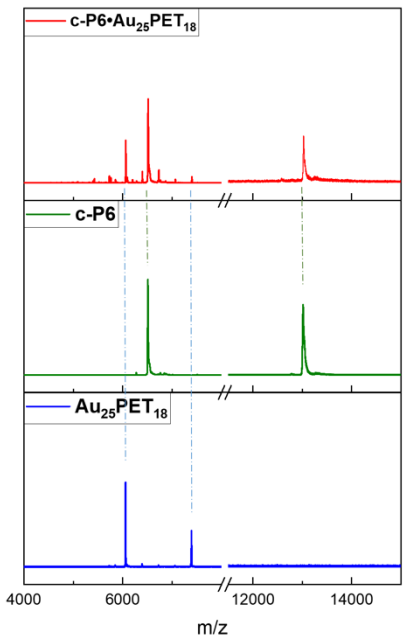

Figure S16. (a) UV-Vis absorption spectra for titration of **$Au_{25}PET_{18}$** and ***c*-P6** and (b) MALDI-MS spectra of **$Au_{25}PET_{18}$**, ***c*-P6** and **$Au_{25}PET_{18}$ / *c*-P6**.

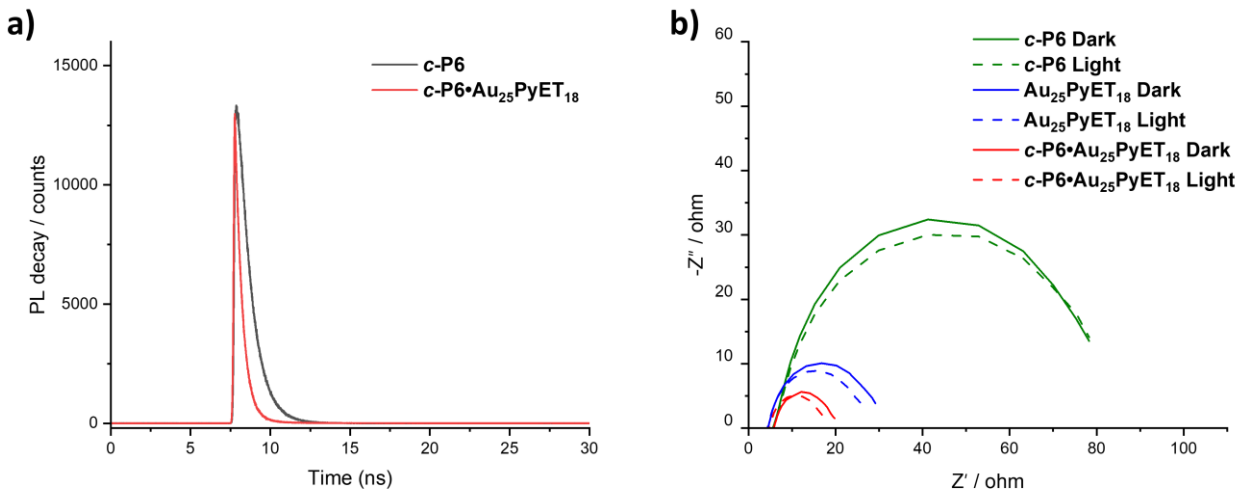

Figure S17. Time-resolved PL spectra of ***c*-P6** and ***c*-P6•Au$_{25}$PyET$_{18}$Na** (a), EIS results of ***c*-P6**, **Au$_{25}$PyET$_{18}$Na** and ***c*-P6•Au$_{25}$PyET$_{18}$Na** under dark and light conditions (b).

Electrocatalytic and photo-coupled electrocatalytic CO_2 reduction

Electrocatalytic CO_2 reduction was conducted with a Metrohm Autolab (PGSTAT302N) station in a homebuilt H-cell (cathodic and anodic compartments are separated by Nafion 117 membrane) equipped with water cooling system in CO_2 saturated 0.5 M $KHCO_3$ (pH = 7.3) under dark condition. Photocoupled electrochemical measurements were performed in the above-mentioned electrochemical system equipped with a 300W Xe lamp. A standard three-electrode configuration was used to conduct electrocatalysis tests: Platinum mesh, Ag/AgCl electrodes and catalyst-modified carbon fiber paper (gas diffusion electrode) were used as the counter and reference electrode and working electrode, respectively. Before experiments, CO_2 gas (99.99%) was purged into the cathode compartment with a flow rate of 20 mL min^{-1} for 30 min under ambient pressure, and then the CO_2 flow rate was controlled at 10 mL min^{-1} for electrocatalytic measurement. Scan rate was 5 mV s^{-1} for linear sweep voltammetry (LSV) in Ar/CO_2-saturated 0.5 M $KHCO_3$. Chronoamperometry was used to perform electrocatalysis at different potentials. Electrochemical impedance spectroscopy (EIS) was performed in CO_2 saturated 0.5 M $KHCO_3$ electrolyte at -0.37 V vs. RHE. In this work, all the electrochemical experiments were performed without *iR* drop correction. The preparation procedures of the working electrode were as follows: 1 mg catalyst and 1 mg carbon black (Vulcan XC-72) were mixed in 50 μL DCM, then 440 μL isopropanol and 10 μL 5wt. % Nafion solution were added, followed by sonication for 30 min, to obtain homogeneous catalyst ink. Then 40 μL ink was dropped directly onto a carbon paper (1 cm × 1 cm) with a catalyst loading density of ~0.08 mg cm^{-2} and dried overnight at room temperature. Reversible hydrogen electrode (RHE) potentials were calculated by the Nernst equation:

$$E_{RHE} = \mathrm{E_{Ag/AgCl}} + 0.197\ V + 0.0591 \times \mathrm{pH}$$

The FE_{CO} was calculated according to the following equation:

$$FE_{CO} = \frac{\mathrm{Q}_{CO}}{\mathrm{Q}_{total}} \times 100\% = \frac{2nF}{\mathrm{Q}_{total}} \times 100\% = \frac{2FV\nu}{V_m I_{total}} \times 100\%$$

In which 2 is the electron transfer number (from CO_2 to CO), n is the molar quantity of CO production, F is the Faradaic constant (96485 C/mol), Q_{total} is the total charge from chronoamperometry, V is CO_2 flow rate (L/s), ν is

volume concentration of CO in H-cell, V_m is molar volume of gas at room temperature, I_{total} is the steady-state current (A).

The turnover frequency (TOF, h^{-1}) of CO was calculated by the equation:

$$TOF = \frac{\mathrm{I}_{total} \times FE_{CO}}{\mathrm{N} \times \mathrm{F} \times \mathrm{n}_{catalyst}} \times 3600$$

Where I_{total} is the total current (A), FE_{CO} is the Faraday efficiency of CO (%), N is electron transfer number (N = 2 for CO_2 to CO conversion), F is the Faraday constant (96485 C/mol), $n_{catalyst}$ is the moles of catalyst coated on the electrode (mol).

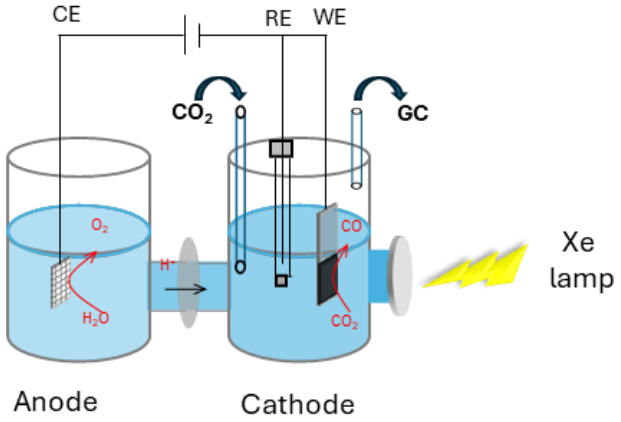

Figure S18. Schematic of photo-electrochemical H-cell.

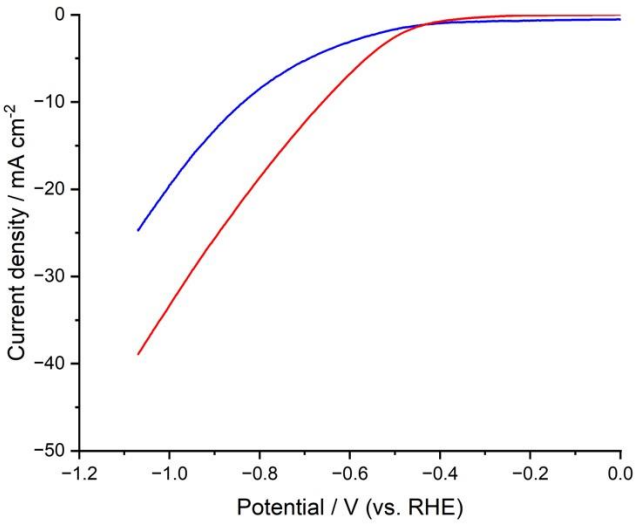

Figure S19. LSV curves of ***c*-P6•Au$_{25}$PyET$_{18}$Na** in N_2- (blue) and CO_2- (red) saturated 0.5 M $KHCO_3$ solution.

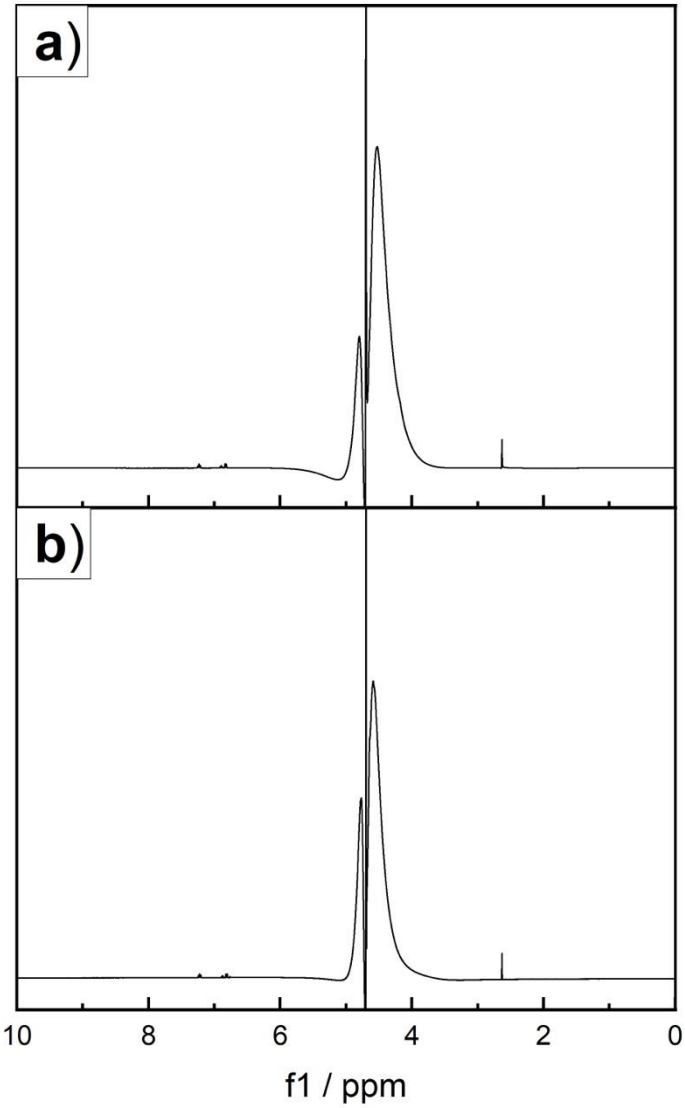

Figure S20. ^{1}H-NMR spectroscopy of electrolyte of ***c*-P6•Au$_{25}$PyET$_{18}$Na** before (a) and after (b) photo-coupled electrocatalytic test at -0.67 V vs. RHE. H-NMR (400 MHz, Bruker) spectra of the electrolyte were measured according to the following method: Aqueous solution of 20 mM phenol and 10 mM dimethyl sulfoxide was prepared as internal standard. After CO_2 reduction reaction, 200 µL D_2O and 50 µL internal standard were added to 350 µL electrolyte and transferred to an NMR tube.

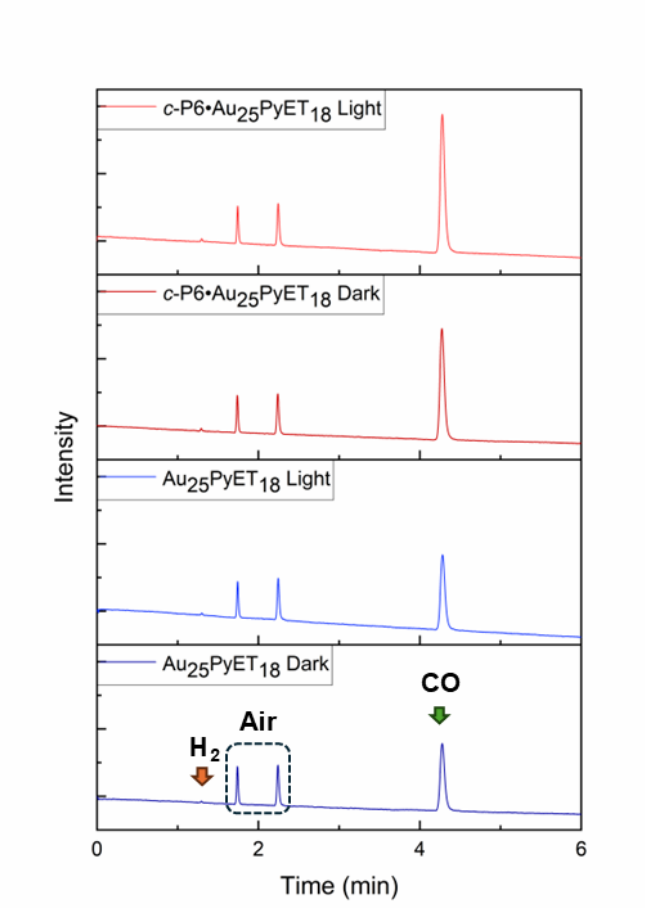

Figure S21. GC results of **$Au_{25}PyET_{18}Na$** and ***c*-P6•$Au_{25}PyET_{18}Na$** under dark and light conditions at -0.67 V vs. RHE.

Table S2. Electrocatalytic CO_2 reduction activities for some of the reported Au-based catalysts.

Catalysts	Selectivity $FE_{CO\ max}$	CO partial current density (mA/cm^2)	Potential vs. RHE (V)	Ref.
$Au_{333}PET_{79}$	~96%	~17	-0.77	[9]
$Au_{44}TBBT_{28}$	82%	~2	-0.57	[10]
$Au_{279}TBBT_{84}$	91%	~17.5	-0.77	[9]
$Au_4(PPh_3)_3I_2$	~75%	~2	-0.7	[11]
$Au_9(PPh_3)_8(NO_3)_3$	~83%	~3	-0.87	[12]
Gold nanoparticles (2nm)	88.8%	-	-0.97	[13]
Gold nanoparticles (5nm)	10.6%	-	-0.97	[13]
$Au_{38}(SCH_2Ph^tBu)_{24}$	~66%	2.5	-0.6	[14]
$Pt_1Au_{37}(SCH_2Ph^tBu)_{24}$	~78%	~7	-0.6	[14]
$Au_{44}(TBBT)_{28}$	~83%	~1.6	-0.57	[15]
This work	92%	10	-0.67	

Singlet oxygen generation

The set-up is similar to the one described in ref. [16] In particular, for irradiation the die of a LED (Thorlabs, 505 nm, LED505L) was imaged onto the sample using a biconvex lens (f = 50 mm). The emission spectrum of the UV-LED, $I_{LED}(\lambda)$, was measured with the set-up described below with the LED light scattered into the absorption path.

The sample (inside a standard 10 × 10 mm^2 fluorescence cuvette) was placed inside a home-built holder, with the LED irradiation being perpendicular to the white light beam path of the absorption spectrometer. The absorption spectrometer consisted of a balanced deuterium-halogen lamp (Avantes, AVALIGHT-DH-S-BAL) and a fiber-optic spec- trometer (Avantes, AVASPEC-ULS2048CL-EVO-RS). The light source was connected to the sample compartment using a 100 µm fiber and a collimating lens (Avantes, COL- UV/VIS), resulting in a total power (over the entire spectrum) of approx. 10 µW, which was sufficiently low to avoid photodecomposition. The sample compartment was con- nected to the spectrometer via a 400 µm fiber. In order to avoid straylight hitting the sample a 7x7 mm^2 blackened mechanical aperture was placed in front of the cuvette (in the LED beampath). The photon flux was measured using a calibrated photodiode-based powermeter (Thorlabs, S120VC) behind the cuvette position (empty and cuvette filled with solvent). The power arriving at the sample was ca. 600 µW

(over the spectrum of the LED). One absorption spectrum comprised the mean of 5 spectra, each taken with an integration time of 0.15 s. Spectra were taken at a time interval of 1.5 s.
The sample solution was stirred and the sample volumes were kept low (≤ 1 mL), such that the entire solution is in quasi-equilibrium.

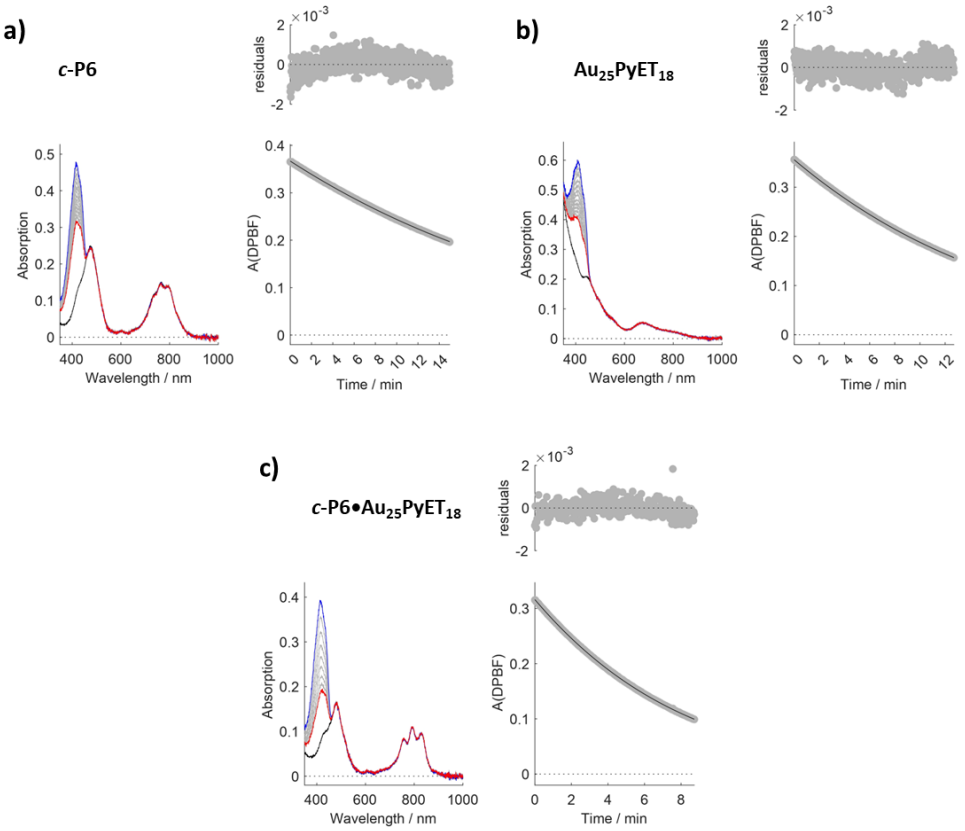

Figure S22. Time dependence of the absorption spectra (left panels), as well as the time dependence of the DPBF maximum absorption (right panels) with a fit to the data and the corresponding residuals. The blue and red spectra denote the first and last recorded absorption spectrum, respectively, for ***c*-P6**, **$Au_{25}PyET_{18}Na$** and ***c*-P6•$Au_{25}PyET_{18}Na$** in THF (a-c).

Chemicals were used as received. Rose bengal (RB, Aldrich 95%) was used as reference system and 1,3-diphenylisobenzofuran (DPBF, Merck, 97%) was used as substrate for the singlet oxygen determination. The solvent (THF) was purged with air for at least 5 min before sample preparation, ensuring air saturation.

All samples are prepared incrementally directly in the cuvette with the cuvette being mounted in the set-up in the following order:

1. solvent only, which serves as background, which is subtracted from all subsequent spectra automatically.
2. adding the stock solution (10 µL) of catalyst, giving rise to $C_{dark}(\lambda)$
3. illuminating this solution with the LED, giving rise to $C_{light}(\lambda)$.[1]
4. with the LED off, adding stock solution of substrate, giving rise to $S(\lambda) = 4 -$

[1] This measurement is important for relatively strongly emissive samples, as emission will leak into the absorption path, thus hampering the spectral decomposition.

$C_{dark}(\lambda)$. For further analysis $S(\lambda)$ was normalized to the maximum.

5. optional, running a time series with the LED off, in order to check for decomposition due to the white-light.
6. with the LED on, record the actual time-series, $A(\lambda, t)$.

The spectra obtained from 2. to 4. were the average of 10 measurements.

Eventually, the spectrotemporal map, $A(\lambda, t)$, can be decomposed into $S(\lambda)$ and $C_{light}(\lambda)$ via a multilinear regression (Matlab, mregress),

$$A(\lambda, t) = s(t) \cdot S(\lambda) + c(t) \cdot C_{light}(\lambda) \quad (1)$$

yielding $s(t)$ and $c(t)$, i. e. the relative contribution of S and C, at each time step t.[2]
From the time dependence of $s(t)$ the singlet oxygen quantum yield of C can be obtained using the kinetic scheme shown in Figure S19. Following the derivation in the supporting information of ref. [17] the following relationship between time and substrate absorption is obtained:

$$t = \underbrace{\frac{V N_A}{\epsilon d N_{abs}}}_{C_1} \frac{1}{\phi_C} \left(\underbrace{\frac{\epsilon d k_0}{k_r}}_{C_2} \ln \frac{s(0)}{s(t)} + \underbrace{\frac{k_r + k_q}{k_r}}_{C_3} (s(0) - s(t)) \right). \quad (2)$$

Here, V is the total sample volume in L, N_A is the Avogadro number, ϵ denotes the substrate's molar extinction coefficient of the maximum of the lowest energy absorption band (here, $\epsilon = 23\,000\ M^{-1}\ cm^{-1}$ at approx. 410 nm) [10] in $M^{-1}\ cm^{-1}$ and d is the pathlength of the probe light in cm.

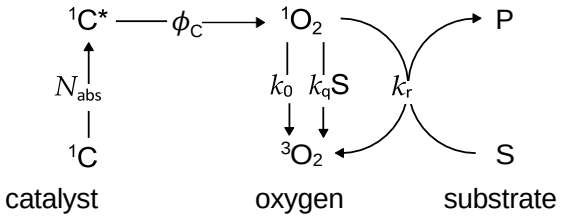

Figure S23. Simplified kinetic scheme of the processes involved in the measurement of the singlet oxygen yield.

The processes of the corresponding rate constants k_i are shown in the kinetic scheme in Figure S20. The number of photons absorbed, N_{abs} is calculated using

$$N_{abs} = \int \left(1 - 10^{\overline{c(t)} C_{dark}(\lambda)}\right) \cdot I_{LED}(\lambda) \cdot P \cdot \lambda \cdot \frac{8065}{1.602 \cdot 10^{-12}} d\lambda,$$

where $I_{LED}(\lambda)$ is the area normalized emission spectrum of the LED, P is the power of the LED (in W), λ is the wavelength (in nm) and $\overline{c(t)}$ is the temporal mean of the catalyst coefficients from the spectral decomposition (to within 1% constant for all cases in this work).

Eq. 2 is fitted to the time-dependence of $s(t)$ using a non-linear least squares optimization (Matlab, lsqnonlin). Given, that ϕ_{RB} in THF is not known we cannot use the prevailing approach of a comparative measurement. Instead - using the condition of $C_3 = 1$, [10] we use a set of three measurements of RB in THF under different

[2] This allows a more precise determination of the substrate absorption, while at the same time monitoring potential (detrimental) changes in the sample

measurement conditions (P, $s(0)$) to determine $\phi_{RB} = 0.60 \pm 0.04$ and $C_2 = 1.49 \pm 0.11$ (see Figure S21).[3] With the average of the so obtained C_2 we fit ϕ_C for the three samples under investigation.
We estimate the error for the quantum yields to be about 10% (relative) of the given value, based on the obtained error for the three independent measurements of RB in THF.

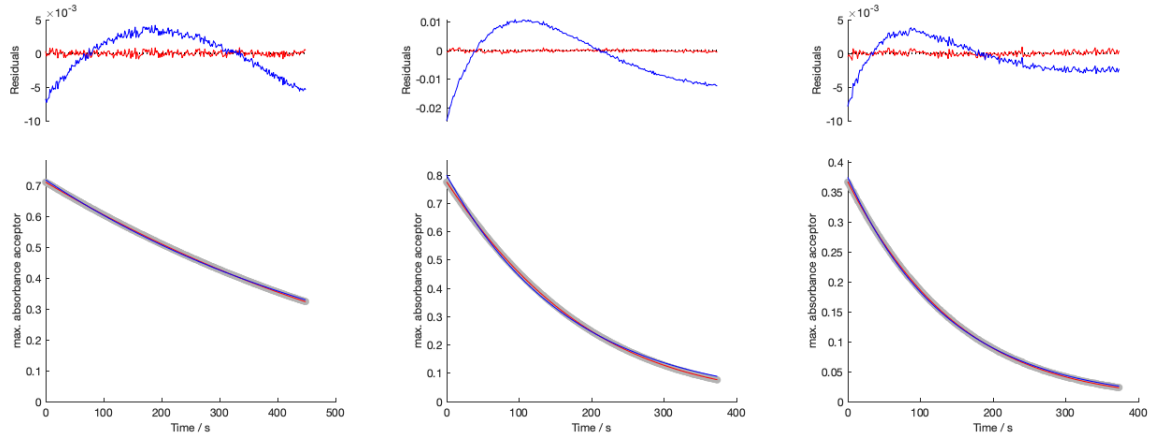

(a) P = 200 µW c(DPBF) = 3×10^{-5} M

(b) P = 600 µW c(DPBF) = 3.4×10^{-5} M

(c) P = 600 µW c(DPBF) = 1.5×10^{-5} M

Figure S24. Decay of the substrate absorption as a function of time (gray points), fits with the model outlined in the Supporting information (red line) and a monoexponential function (blue line), and the corresponding residuals (upper panels).

[3] Whenever the kinetics are governed by the 1st order contribution (i. e. when the first term in the parenthesis in eq. (2) prevails over the second term) the two fitting parameters ϕ_C and C_2 are strongly correlated.

References

[1] M. Hoffmann, J. Kärnbratt, M. H. Chang, L. M. Herz, B. Albinsson, H. L. Anderson *Angew. Chem. Int. Ed.* **2008**, *47*, 4993-4996.

[2] D. V. Kondratuk, L. M. Perdigão, A. M. Esmail, J. N. O'shea, P. H. Beton, H. L. Anderson, *Nat. Chem.* **2015**, *7*, 317-322.

[3] S. Liu, D. V. Kondratuk, S. A. Rousseaux, G. Gil-Ramírez, M. C. O'Sullivan, J. Cremers, T. D. Claridge, H. L. Anderson, *Angew. Chem. Int. Ed.* **2015**, *54*, 5355-5359.

[4] Z. Huang, Y. Ishida, T. Yonezawa, *Angew. Chem. Int. Ed.* **2019**, *58*, 13411-13415.

[5] Y. Wang, T. Bürgi, *Nanoscale* **2022**, *14*, 2456-2464.

[6] J. Zhao, A. Ziarati, A. Rosspeintner, Y. Wang, T. Bürgi, *Chem. Sci.* **2023**, *14*, 7665-7674.

[7] B. Walfort, N. Gartmann, J. Afshani, A. Rosspeintner, H. Hagemann, *J. Rare Earth* **2022**, *40*, 1022-1028.

[8] J. K. Sprafke, D. V. Kondratuk, M. Wykes, A. L. Thompson, M. Hoffmann, R. Drevinskas, W.-H. Chen, C. K. Yong, J. Karnbratt, J. E. Bullock, *J. Am. Chem. Soc.* **2011**, *133*, 17262-17273.

[9] S. Li, A. V. Nagarajan, X. Du, Y. Li, Z. Liu, D. R. Kauffman, G. Mpourmpakis, R. Jin, *Angew. Chem. Int. Ed.* **2022**, 61, e202211771.

[10] S. Zhuang, D. Chen, W.-P. Ng, L.-J. Liu, M.-Y. Sun, D. Liu, T. Nawaz, Q. Xia, X. Wu, Y.-L. Huang, S. Lee, J. Yang, J. Yang, J. He, *Angew. Chem. Int. Ed.* **2023**, 62, e202306696.

[11] C. Zhang, M. Ding, Y. Ren, A. Ma, Z. Yin, X. Ma, S. Wang, *Nanoscale Adv.* **2023**, 5, 3287.

[12] S. K. Sharma, H. T. Ahangari, B. Johannessen, V. B. Golovko, A. T. Marshall, *Electrocatalysis* **2023**, 14, 611.

[13] D. R. Kauffman, D. Alfonso, C. Matranga, H. Qian, R. Jin, *J. Am. Chem. Soc.* **2012**, 134, 10237.

[14] X. Liu, E. Wang, M. Zhou, Y. Wan, Y. Zhang, H. Liu, Y. Zhao, J. Li, Y. Gao, Y. Zhu, *Angew. Chem. Int. Ed.* **2022**, 61, e202207685.

[15] S. Zhuang, D. Chen, L. Liao, Y. Zhao, N. Xia, W. Zhang, C. Wang, J. Yang, Z. Wu, *Angew. Chem. Int. Ed.* **2020**, 59, 3073.

[16] Q. H. a. E. R. H. Volfova, *EPA Newsletter* **2019**, 51-69.

[17] T. Entradas, S. Waldron, M. Volk, *J. Photochem. Photobiol. B* **2020**, *204*, 111787.